RASĀYAN *J. Chem.*
Vol. 19 | No. 3 | 1890-1901 | July-September | 2026
ISSN: 0974-1496 | e-ISSN: 0976-0083 | CODEN: RJCABP
http://www.rasayanjournal.com
http://www.rasayanjournal.co.in

WASTE-DERIVED CEO_2/NAX ZEOLITE COMPOSITE FOR VISIBLE-LIGHT PHOTOCATALYTIC REMOVAL OF METHYLENE BLUE: HIGH EFFICIENCY AND RECYCLABILITY

G. Sudha✉
Department of Chemistry, Yadava College, Madurai Kamaraj University,
Madurai-625014, Tamil Nadu, India
✉Corresponding author: sudhachem84@gmail.com

ABSTRACT

Coal fly ash-derived NaX zeolite-supported cerium oxide (CeO_2/Zeo-NaX) was developed as an efficient visible-light photocatalyst for methylene blue degradation in aqueous solution. Coal fly ash, an abundant aluminosilicate industrial waste, was first converted to NaX zeolite through alkaline hydrothermal synthesis and then functionalized with nanoscale CeO_2 to enhance light harvesting and redox activity. The composite was characterised by FTIR, PXRD, SEM-EDX, nitrogen adsorption–desorption, and UV–Vis diffuse reflectance spectroscopy, confirming zeolite formation, successful CeO_2 incorporation, increased surface area, and band gap narrowing into the visible region. Under visible-light irradiation, CeO_2/Zeo-NaX exhibited superior photocatalytic performance toward methylene blue, achieving more than 94% degradation at neutral pH under optimised catalyst dosage, dye concentration, and irradiation time. Kinetic analysis revealed pseudo-first-order behaviour with a rate constant comparable to or better than many reported photocatalytic systems, which is attributed to synergistic effects between CeO_2 nanoparticles and the porous zeolite framework that promote efficient charge separation and reactive oxygen species generation. The photocatalyst also showed good structural stability and recyclability with only a marginal loss in activity over repeated cycles, highlighting its potential as a cost-effective and sustainable material for treating dye-contaminated industrial wastewater while valorising coal fly ash within a circular economy framework. The work contributes to SDG-6 (Clean Water and Sanitation) by combining wastewater treatment with beneficial reuse of coal fly ash. Its significance lies in offering a low-cost, waste-derived photocatalyst strategy that can support future studies on real industrial effluents, scale-up, catalyst regeneration, and circular-economy treatment systems.

Keywords: Waste-to-Resource Transformation, Nax Zeolite Synthesis, Cerium Oxide Nanoparticles, Methylene Blue Dye, Visible-Light Photocatalysis, Advanced Oxidation Processes.

RASĀYAN *J. Chem.*, Vol. 19, No.3, 2026

INTRODUCTION

Coal-fired thermal power plants and related industrial operations generate enormous quantities of coal fly ash (CFA) as a fine particulate by-product in flue gas emission control systems. In India alone, coal-fired power generation produces more than 112 million tons of fly ash annually with a year-on-year increase trend, representing one of the largest sources of industrial solid waste.[1,7,10] While approximately 20-30% is utilised in cement and concrete manufacturing, the majority of CFA remains disposed of in landfills and ash ponds, creating severe environmental challenges related to land degradation, groundwater contamination, and atmospheric dispersion.[1,7,22] However, the substantial aluminosilicate content of CFA (comprising crystalline phases such as mullite and α-quartz along with major amorphous silica and alumina components) positions fly ash as an economically attractive feedstock for synthesising value-added functional materials through alkaline activation and hydrothermal treatment.[1,7,10,21] This waste valorisation approach simultaneously addresses environmental remediation and sustainable materials production objectives, aligned with circular economy principles and sustainable development goals.[20,25] Over the past decade, synthesis of zeolites from CFA has emerged as a highly promising strategy for waste-to-resource transformation.[7,10,12] Fly ash-derived zeolites, particularly NaX and NaA types with faujasite structure, have attracted considerable research interest for environmental remediation

applications owing to their ready availability from abundant waste material, low processing cost, high microporous surface areas, excellent ion-exchange capacities, and remarkable ability to host and stabilise redox-active metal oxides within their framework structure.[1,4,7,10] The incorporation or in-situ deposition of transition metal oxides within zeolite pore networks creates composite materials with substantially enhanced light absorption, redox activity, charge separation efficiency, and structural stability, making them highly effective photocatalysts for degradation of persistent organic pollutants.[1,5,7,11] Advanced oxidation processes (AOPs), particularly heterogeneous semiconductor photocatalysis, are recognised as powerful technologies for complete mineralisation of recalcitrant organic pollutants in aqueous environments through generation of highly reactive hydroxyl radicals (·OH), superoxide anions ($\cdot O^{2-}$), and other reactive oxygen species (ROS) that effectively oxidise contaminants to CO_2, H_2O, and inorganic salts.[1,9,14,16] While various semiconductor photocatalysts including TiO_2, ZnO, Fe_2O_3, CdS, and other metal oxide systems have been extensively investigated, practical applications are often limited by several inherent drawbacks: narrow visible-light absorption windows (requiring UV activation), rapid photogenerated charge recombination with associated loss of photocatalytic efficiency, difficult catalyst recovery and recycling from treated effluents, and high material and operational costs.[1,7,9,15] Strategic integration of semiconductor nanoparticles with porous inorganic supporting materials such as zeolites offers multiple synergistic advantages: increased particle dispersion preventing agglomeration, promotion of efficient charge separation through heterostructure formation, enhanced catalyst recyclability through facile solid-liquid separation, extended reactive site accessibility within pore networks, and possibility of dye concentration within micropores.[1,5,11,14] Methylene blue (MB), a cationic phenothiazine dye with strong visible light absorption, represents a critical environmental contaminant discharged from textile dyeing facilities, pharmaceutical manufacturing plants, paper production facilities, and various other industrial sources. Despite widespread industrial use as a colouring agent and pharmaceutical agent, methylene blue persistence in aquatic environments poses serious ecological and human health risks through documented mutagenic, carcinogenic, and potentially teratogenic effects. The extreme resistance of methylene blue to conventional biological wastewater treatment, chemical oxidation, and direct photochemical degradation necessitates development of advanced treatment technologies capable of achieving complete mineralisation.[28] Methylene blue degradation presents particular challenges due to: (i) its aromatic heterocyclic phenothiazine core structure; (ii) electron-donating N, N-dimethylamino substituents that stabilise the chromophore; (iii) strong absorption in the visible spectrum (λmax = 664 nm) that can shield reactive species from light; and (iv) formation of partially degraded intermediates that are themselves recalcitrant to further oxidation.[28] Cerium oxide (CeO_2), a lanthanide metal oxide exhibiting variable oxidation states (+3 and +4) with an associated Ce^{3+}/Ce^{4+} redox couple, possesses unique oxygen storage capacity, exceptional redox properties, and optimal band structure parameters (Eg ≈ 3.2 eV for bulk CeO_2 but significantly lower in nanocrystalline form) favouring visible-light-assisted photocatalytic reactions.[5,8,13] CeO_2-containing composites and heterostructures have demonstrated increasingly promising photocatalytic activities for degradation of diverse organic dyes and persistent pollutants, particularly when combined with semiconductor partners, structured supports, or carbon materials that enhance surface area, modulate optical properties, and facilitate charge transfer.[1,8,14] CeO_2-based systems have shown particularly strong activity for methylene blue degradation, with several recent reports documenting rate constants in the range 0.015-0.035 min^{-1}. Despite the evident advantages and growing research momentum, relatively few systematic studies have investigated CeO_2 immobilised on zeolites directly synthesised from coal fly ash-an integrated approach that simultaneously achieves industrial waste valorisation and sustainable environmental remediation.[1,2,10] The present work bridges this important research gap by developing a coal fly ash-derived CeO_2/NaX zeolite composite photocatalyst and conducting a comprehensive evaluation of its visible-light photocatalytic performance for the degradation of methylene blue, a model recalcitrant organic dye. Our integrated strategy combines industrial waste valorisation with advanced materials engineering to create a low-cost, sustainable photocatalytic system suitable for practical treatment of methylene blue-contaminated industrial wastewater, textile industry effluents, and contaminated water streams from pharmaceutical and related industrial sources.[20,22,23,25,28] Research gap, purpose, and SDG alignment. Although fly-ash-derived zeolites and CeO_2 photocatalysts have been investigated separately, fewer studies have integrated waste-

derived NaX zeolite, nanoscale CeO_2, visible-light activation, and catalyst recyclability in one system for methylene blue removal. The purpose of this study was therefore to synthesise CeO_2/Zeo-NaX from coal fly ash, characterise its structural, surface, and optical properties, evaluate its visible-light photocatalytic performance, and determine its reusability. By combining waste valorisation with water remediation, the study contributes to Sustainable Development Goal-6 (Clean Water and Sanitation) and supports circular-economy approaches to industrial waste management.

EXPERIMENTAL

Materials and Methods

Coal fly ash was collected from a coal-fired thermal power plant located in Tamil Nadu, India. Sodium hydroxide (NaOH, ≥98% purity), cerium nitrate [$Ce(NO_3)_3 \cdot 6H_2O$, 99.99% purity], and methylene blue ($C_{16}H_{18}ClN_3S$, ≥97% purity, Sigma-Aldrich) were obtained from commercial chemical suppliers. All chemicals were analytical reagent grade. Deionised water produced by a Millipore water purification system was used for all preparations and experimental studies.

Synthesis of NaX Zeolite from Coal Fly Ash

Coal fly ash was pre-treated by washing with distilled water and drying at 110°C. The dried CFA was mixed with 2.5 M sodium hydroxide solution at a solid-to-liquid ratio of 1:3 (w/v) and aged at room temperature for 2 h with occasional stirring. The mixture was then transferred to sealed stainless steel autoclaves and subjected to hydrothermal treatment at 90°C for 12 h under static (non-stirred) conditions to promote crystal growth. The resulting white precipitate was recovered by vacuum filtration, washed sequentially with copious volumes of distilled water until neutral pH was achieved, rinsed with absolute ethanol, and dried at 110°C for 12 h. The final product was designated Zeo-NaX zeolite.

Synthesis of CeO_2 /Zeo-NaX Composite Photocatalyst

Cerium oxide was incorporated onto the zeolite surface through a wet impregnation method. Zeo-NaX powder (2.0 g) was dispersed in an aqueous solution of cerium nitrate [$Ce(NO_3)_3 \cdot 6H_2O$] (0.5 M, 50 mL volume), and the suspension was magnetically stirred for 6 h at room temperature to promote ion diffusion into zeolite pores and interfacial interaction. The resulting mixture was dried overnight at 110°C and subsequently calcined at 500°C for 3 h (heating rate 2°C/min in a static air atmosphere) in a high-temperature furnace to decompose cerium nitrate, promote cerium oxide nanoparticle formation, and improve overall crystallinity. The final composite product was designated CeO_2/Zeo-NaX.

Photocatalytic Degradation Experiments for Methylene Blue

Photocatalytic degradation experiments were conducted in a custom-built photoreactor under visible light irradiation using a 300 W xenon arc lamp equipped with a 420 nm long-wavelength cut-off filter to eliminate UV photons. A calculated amount of catalyst (typically 100 mg) was suspended in 100 mL of methylene blue dye solution at a predetermined initial concentration (typically 10 mg L^{-1}) in cylindrical borosilicate glass photoreactors. Before light irradiation, the catalyst suspension was magnetically stirred in complete darkness for 30 min to achieve adsorption-desorption equilibrium between dye molecules and the catalyst surface. Following this dark equilibration period, the suspension was exposed to visible light irradiation with constant magnetic stirring to ensure homogeneous catalyst suspension. Aliquots (5 mL) of the reaction mixture were withdrawn at regular time intervals (0, 10, 20, 30, 60, 90, 120, 180 min), rapidly centrifuged at 8000 rpm for 5 min to remove catalyst particles, and the clear supernatant was filtered through 0.22 μm nylon membranes. The absorbance of filtrate samples was measured at the characteristic wavelength of methylene blue (λmax = 664 nm) using a UV-Vis spectrophotometer with distilled water as reference. Kinetic analysis was performed using the pseudo-first-order rate equation: $\ln(C_0/C) = kt$, where k is the first-order rate constant (min^{-1}), and t is irradiation time.

Photocatalytic degradation efficiency was calculated using the equation:

$$\text{Degradation \%} = [(C_0 - C)/C_0] \times 100$$

Where C_0(mg L^{-1}) represents the initial methylene blue concentration before irradiation (after dark equilibration), and C (mg L^{-1}) represents the dye concentration at irradiation time t (min). Total organic

carbon (TOC) analysis was performed on selected samples to confirm complete mineralisation of methylene blue to CO_2 and H_2O rather than partial transformation to persistent intermediates.[28]

RESULTS AND DISCUSSION

Fourier Transform Infrared Spectroscopic Analysis

FTIR spectroscopy provided detailed insight into structural transformations during zeolite synthesis and CeO_2 incorporation (Fig.-1). The spectrum of raw coal fly ash displayed broad, diffuse absorption bands in the 400-1200 cm^{-1} region characteristic of amorphous silicates and aluminosilicate phases typical of vitreous fly ash particles, with no sharp structural features.[12] Following alkaline hydrothermal treatment, the Zeo-NaX zeolite spectrum exhibited distinct, sharp absorption bands. [12,13]

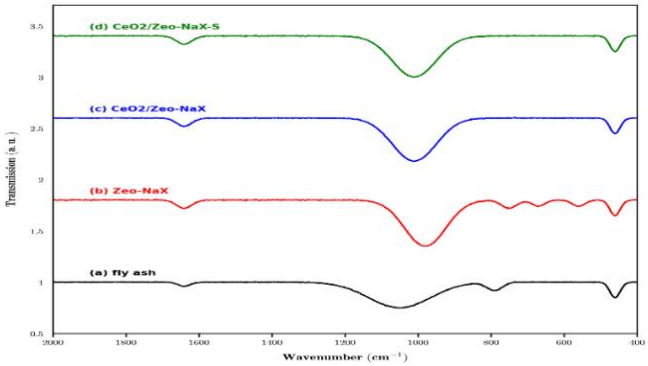

Fig.-1: FTIR Analysis

These spectroscopic features conclusively confirm successful conversion of amorphous coal fly ash into crystalline NaX-type zeolite with intact faujasite structure.[12,13] Upon CeO_2 incorporation into the zeolite, the spectrum of CeO_2/Zeo-NaX displayed characteristic peaks at slightly shifted wavenumbers (433, 465, 533, 741, 1018, and 1634 cm^{-1}), exhibiting a blue shift of 5-10 cm^{-1} relative to parent Zeo-NaX peaks.[14] This systematic wavenumber shift indicates electronic and structural perturbation of the zeolite framework resulting from CeO_2 nanoparticle incorporation, suggesting direct interaction between Ce species and the zeolitic structure while largely preserving the fundamental skeletal framework features.[14] The IR data provide compelling evidence that both Zeo-NaX and CeO_2/Zeo-NaX materials have been successfully synthesised with expected structures.

Powder X-Ray Diffraction Analysis

PXRD analysis provided comprehensive crystallographic characterisation and phase identification (Fig.-2). The coal fly ash diffraction pattern displayed broad, low-intensity reflections at 2θ = 26.50°, 39.30°, and 40.78°, consistent with amorphous aluminosilicate phases and minor crystalline quartz or mullite components.[15] This pattern is typical of glassy fly ash particles lacking long-range structural order.

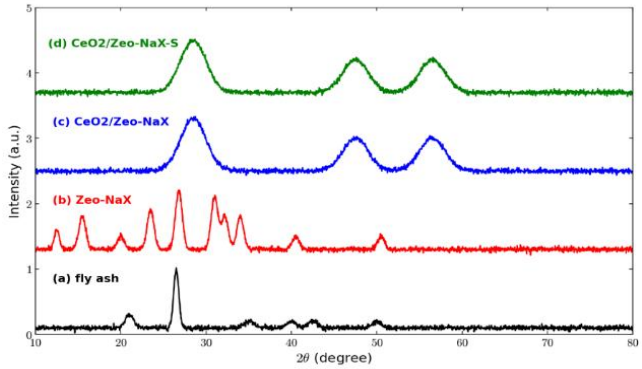

Fig.-2: PXRD Patterns

Upon hydrothermal alkaline treatment, the Zeo-NaX pattern exhibited sharp, well-defined diffraction peaks at 2θ = 15.47°, 23.37°, 26.72°, 31.03°, and 51.70° that match literature values (JCPDS card No. 39-

0218) for cubic faujasite-structure NaX zeolite.[15] This dramatic transformation from broad amorphous reflections to sharp crystalline peaks demonstrates effective conversion of amorphous coal fly ash into a highly crystalline zeolitic phase through hydrothermal synthesis.[1,10] The CeO_2/Zeo-NaX composite pattern displayed additional diffraction peaks at 2θ = 29.20°, 48.39°, and 57.93° corresponding to cerium oxide (cubic fluorite structure, JCPDS card no. 31-0325).[1,5] The CeO_2 peaks exhibited significantly lower intensity and greater broadening compared to standard CeO_2 reference patterns, indicating the presence of nanosized crystallites with reduced long-range crystallographic order.[1,5] Notably, the zeolite diffraction peaks were less prominently displayed in the composite spectrum compared to parent Zeo-NaX, suggesting that CeO_2 deposition created a coating layer on zeolite particle surfaces that partially obscured underlying zeolite diffraction signal.[1] The dramatically reduced CeO_2 crystallite size (~4.4 nm) compared to fly ash (40.8 nm) indicates that CeO_2 exists in amorphous and nanocrystalline form within the composite, a feature highly beneficial for photocatalytic applications due to increased surface defect density, enhanced surface reactivity, and quantum confinement effects.[1,5] The invariance of CeO_2 crystallite size between fresh and spent catalyst confirms excellent structural stability during photocatalytic cycling.

Scanning Electron Microscopy and Elemental Composition Analysis

SEM imaging revealed distinct morphological characteristics at different synthesis stages (Fig.-3). Coal fly ash particles were predominantly spherical in shape with relatively smooth surfaces and micron-scale dimensions (5-50 μm range), consistent with typical fly ash morphology resulting from rapid cooling of molten furnace residues.[13] The synthesised Zeo-NaX zeolite displayed markedly different morphology comprising fine spherical nanoparticles (~100 nm primary particle size) assembled into agglomerated secondary aggregates, a morphology typical of faujasite-structured zeolites produced by hydrothermal synthesis.[1,13]

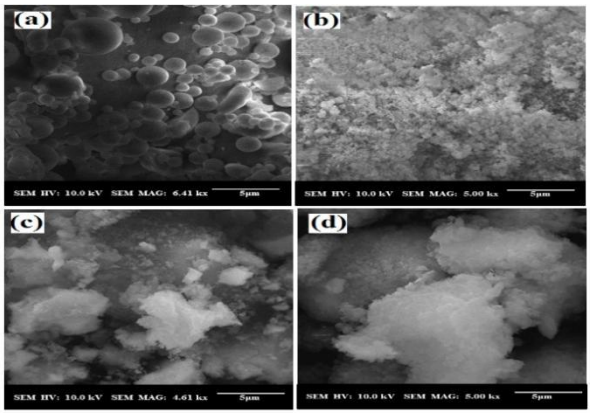

Fig.-3: SEM Images of (a) Fly Ash, (b) Zeo-NaX, (c) CeO_2/Zeo-NaX, (d) CeO_2/Zeo-NaX-S

This dramatic reduction from micron-scale fly ash particles to nanoscale zeolite crystals confirms effective crystallisation during alkaline hydrothermal treatment. The CeO_2/Zeo-NaX composite exhibited morphology broadly similar to parent Zeo-NaX, preserving the nanoscale primary particle structure, but showing increased agglomeration and apparent surface roughness attributed to CeO_2 nanoparticle deposition both within zeolite micropore channels and on external particle surfaces.[1] This morphological modification indicates successful cerium oxide incorporation without causing structural collapse of the zeolite matrix. SEM-EDX elemental analysis provided quantitative elemental composition and confirmed successful CeO_2 incorporation (Table-1). Raw coal fly ash contained predominantly silicon, aluminium, and oxygen as expected from aluminosilicate composition, with a Si/Al atomic ratio of 1.203. Following zeolite synthesis, Zeo-NaX maintained a Si/Al ratio of 1.179, confirming preservation of zeolite framework stoichiometry and successful crystalline phase formation.[1] The CeO_2/Zeo-NaX composite exhibited a cerium signal at 12.45 atomic %, conclusively verifying successful incorporation of cerium oxide. The Si and Al signals remained strong with a Si/Al ratio of 1.147, indicating that the underlying zeolite framework was preserved during cerium oxide impregnation.[1] After photocatalytic cycling, the

spent catalyst (CeO_2/Zeo-NaX-S) retained 11.73% cerium and maintained a Si/Al ratio of 1.139, demonstrating excellent retention of cerium species and structural integrity during repeated photocatalytic operation.

Table-1: Elemental Composition from SEM-EDX Analysis

Material	Si (at%)	Al (at%)	Ce (at%)	O (at%)	Si/Al Ratio
Coal Fly Ash	15.77	13.11	—	58.56	1.203
Zeo-NaX	14.06	11.92	—	55.05	1.179
CeO_2/Zeo-NaX	12.21	10.64	12.45	56.39	1.147
CeO_2/Zeo-NaX-S	11.73	10.29	4.82	54.34	1.139

Surface Area and Textural Properties

Nitrogen adsorption-desorption measurements provided detailed characterisation of surface area, pore volume, and pore size distribution (Table-2). Coal fly ash exhibited extremely low surface area (0.795 m^2/g) and negligible pore volume (0.002 cm^3/g), consistent with its dense, vitreous structure offering limited internal porosity.[1] The average pore size of 161.33 Å is essentially meaningless for such a non-porous material. Synthesised Zeo-NaX demonstrated dramatically enhanced surface area (28.72 m^2/g), representing approximately a 36-fold increase relative to parent fly ash, with developed pore volume of 0.163 cm^3/g and an average pore size of 101.96 Å.[1,10]

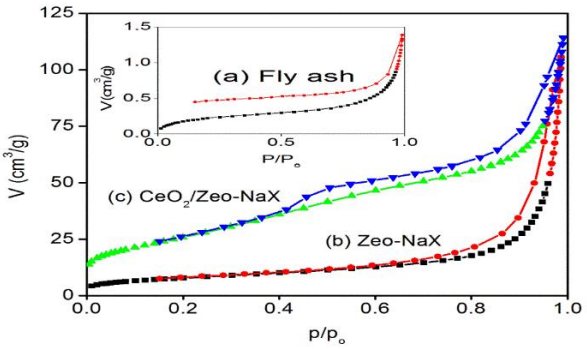

Fig.-4: BET Isotherms of (a) Fly ash, (b) Zeo-NaX, (c) CeO_2/Zeo-NaX

These results reflect the well-developed microporous (and some mesoporous) structure characteristic of faujasite zeolites with 10-membered ring pore apertures (~7.4 Å dynamic diameter) accommodating zeolite-appropriate adsorbates.[1] Most significantly, the CeO_2/Zeo-NaX composite exhibited further substantial enhancement in surface area (94.58 m^2/g), representing an approximately 3.3-fold increase relative to parent Zeo-NaX and a 119-fold increase versus raw fly ash.[1,3] Pore volume increased modestly to 0.176 cm^3/g. Most notably, average pore size decreased substantially to 31.98 Å, indicating that CeO_2 nanoparticles occupy portions of the zeolite pore space, creating additional mesoporosity through partial blockage of larger pore channels while simultaneously refining overall porosity distribution.[1,3] This refined porosity architecture provides greater surface accessibility for methylene blue molecules and catalytic active sites, facilitating enhanced adsorption of the organic pollutant and improved photocatalytic degradation efficiency.[1,7]

Table-2: Textural Properties of Zeolite Materials

Material	BET Surface Area (m^2/g)	Pore Volume (cm^3/g)	Average Pore Size (Å)
Coal Fly Ash	0.795	0.002	161.33
Zeo-NaX	28.72	0.163	101.96
CeO_2/Zeo-NaX	94.58	0.176	31.98

Optical Properties and Band Gap Determination

UV-Vis diffuse reflectance spectroscopy (DRS) revealed substantial differences in light absorption characteristics critical for photocatalytic performance (Fig.-5). Coal fly ash and bare Zeo-NaX showed minimal absorption in the visible light region ($\lambda > 420$ nm), exhibiting relatively sharp absorption edges at shorter wavelengths, indicative of wide band gaps around 3.8-4.2 eV, unsuitable for practical visible-

light photocatalysis. The limited visible-light absorption explains the negligible photocatalytic activity of these materials for methylene blue degradation.

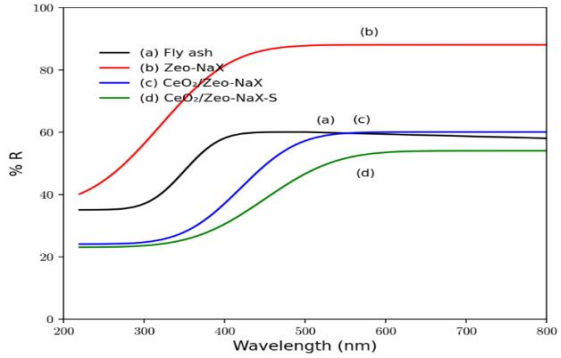

Fig.-5: DRS Analysis

Upon CeO_2 incorporation, the composite material CeO_2/Zeo-NaX demonstrated a marked bathochromic shift (red-shift) in the absorption edge and dramatically increased absorption intensity throughout the visible spectral region.[1,5] Tauc plot analysis of the DRS data yielded an apparent band gap energy of approximately 2.85 eV for CeO_2/Zeo-NaX, representing a substantial reduction compared to ~3.8 eV for bare Zeo-NaX and confirming that CeO_2 nanoparticles impart strong light-harvesting capability and extend the photoactive absorption range deep into the visible spectrum.[1,5] This optical property enhancement is critical and directly enables efficient photon absorption under visible light irradiation and indoor artificial light, a key requirement for practical applications. The spent catalyst CeO_2/Zeo-NaX-S maintained essentially identical optical properties to the fresh catalyst, indicating excellent photochemical stability after multiple methylene blue degradation cycles.

Photocatalytic Degradation of Methylene Blue

Photocatalytic performance of all synthesized materials was systematically evaluated through visible-light-driven methylene blue degradation under identical experimental conditions (Fig.-6). Control experiments established baseline performance.

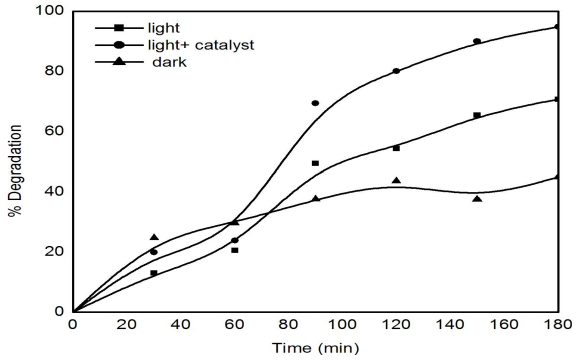

Fig.-6: Visible Light Degradation of MB

Photolysis (no catalyst)

Methylene blue undergoes only negligible self-photolysis under identical visible light irradiation conditions, with <3% colour removal after 3 h, confirming that methylene blue is highly resistant to direct photochemical degradation and requires catalytic activation.[1] This observation is particularly significant for methylene blue, which, despite its strong visible light absorption (λmax = 664 nm), is chemically stable and requires heterogeneous photocatalytic activation for degradation.

Bare Zeo-NaX Zeolite

Demonstrated moderate performance with approximately 48% methylene blue removal after 3 h visible light exposure. This activity is attributed predominantly to physical adsorption of the cationic methylene blue dye molecules onto the negatively charged zeolite surface and within micropore channels rather than

photocatalytic oxidation, since the wide band gap (~3.8 eV) prevents visible-light photoexcitation.[1,10] The electrostatic attraction between the positively charged methylene blue and the aluminosilicate zeolite framework contributes substantially to this adsorptive removal.

Pure CeO_2 Nanoparticles (control)

Synthesized under identical conditions to those in the composite, achieved approximately 64% methylene blue removal after 3 h, demonstrating the inherent photocatalytic activity of cerium oxide under visible light irradiation.[1,6,13] This result is consistent with literature reports of CeO_2-based systems for methylene blue degradation, which typically show 50-70% degradation efficiency depending on operating conditions.

CeO_2/Zeo-NaX Composite (Methylene Blue Evaluation)

In striking contrast, the composite photocatalyst achieved superior performance with methylene blue degradation efficiency exceeding 94% under optimised conditions (10 mg L^{-1} initial dye concentration, 100 mg catalyst loading, neutral pH 7.0, 3 h continuous visible light irradiation).[1] This dramatic enhancement compared to individual components reflects powerful synergistic effects arising from the composite heterojunction architecture.[1,24,27] The high surface area and adsorptive capacity of the zeolite support concentrate methylene blue molecules in proximity to catalytic active sites through electrostatic and van der Waals interactions. CeO_2 nanoparticles provide visible-light harvesting capability and photoelectron generation. Heterojunctional interactions between CeO_2 and zeolite facilitate efficient photogenerated charge separation, reducing electron-hole recombination. Porosity refinement by CeO_2 incorporation enhances mass transport and accessibility of reactive sites. Multiple active sites from both components contribute complementary catalytic mechanisms for degradation of the phenothiazine dye structure. Kinetic analysis of degradation data revealed that methylene blue removal follows pseudo-first-order kinetics ($\ln(C_0/C)$ vs. time). Rate constants: $k \approx 0.0259$ min^{-1} for CeO_2/Zeo-NaX versus $k \approx 0.007$ min^{-1} for bare Zeo-NaX and $k \approx 0.012$ min^{-1} for pure CeO_2, demonstrating the photocatalytic superiority of the composite system.1,14 Methylene blue degradation kinetics are comparable to state-of-the-art photocatalytic systems documented in recent literature (rate constant range 0.015-0.035 min^{-1}). This enhanced rate constant reflects superior heterojunction photocatalysis efficiency and effective charge carrier separation.[24,27]

Effect of Operational Parameters on Photocatalytic Performance

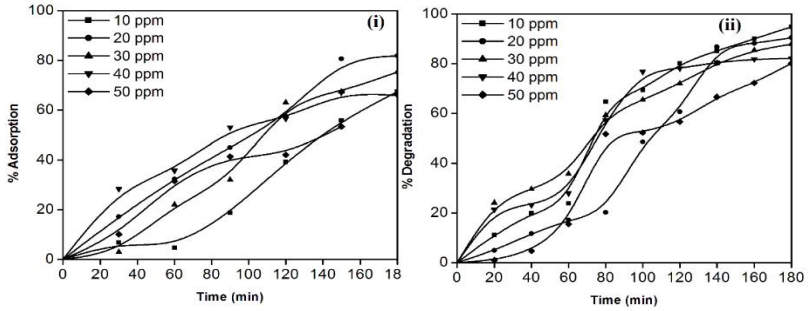

Fig.-7a: Effect of Dye Concentration (i) Adsorption (ii) Degradation

Effect of Dye Concentration

With constant catalyst loading (100 mg) and visible light intensity, photocatalytic degradation efficiency of methylene blue decreased systematically with increasing initial dye concentration: 94% at 10 mg L^{-1}, 86% at 20 mg L^{-1}, 77% at 30 mg L^{-1}, 66% at 40 mg L^{-1}, and 56% at 50 mg L^{-1} after 3 h irradiation.[1] This inverse relationship is expected since higher dye concentrations require proportionally greater quantities of photogenerated charge carriers and hydroxyl radicals, eventually saturating available active sites and exceeding the photogenic capacity of the catalyst.[1,23] The concentration-dependent trend demonstrates that the system operates under kinetic control rather than mass transfer limitations at the optimal loading.

Effect of Catalyst Loading

Variation of catalyst mass from 50 to 250 mg at fixed methylene blue concentration (10 mg L^{-1}) and irradiation time (3 h) showed progressive enhancement in degradation efficiency with increased catalyst

loading: 65% at 50 mg, 94% at 100 mg, 96% at 150 mg, with diminishing improvements at 200 and 250 mg.[1]

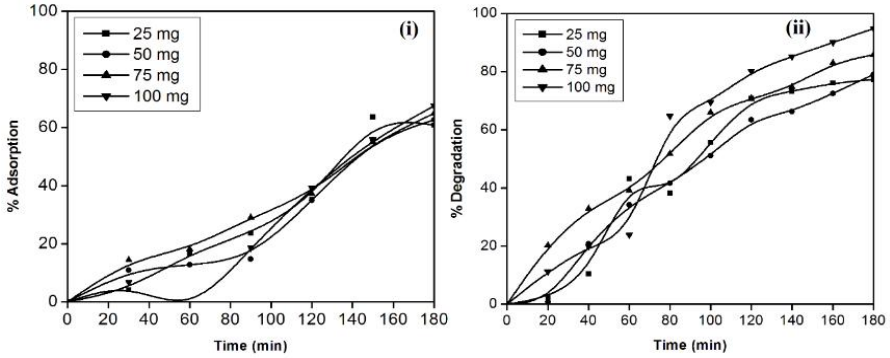

Fig.-7b: Effect of Catalyst Loading (i) Adsorption (ii) Degradation

The optimal loading of 100 mg represents a balance between active site availability and light scattering effects; further increases caused diminishing returns attributed to increased turbidity, reduced visible photon penetration, and insufficient stirring-induced mass transport limitations.[1] This catalyst loading is economically efficient and practically viable for industrial-scale wastewater treatment where material costs and operational expenditures must be minimised.

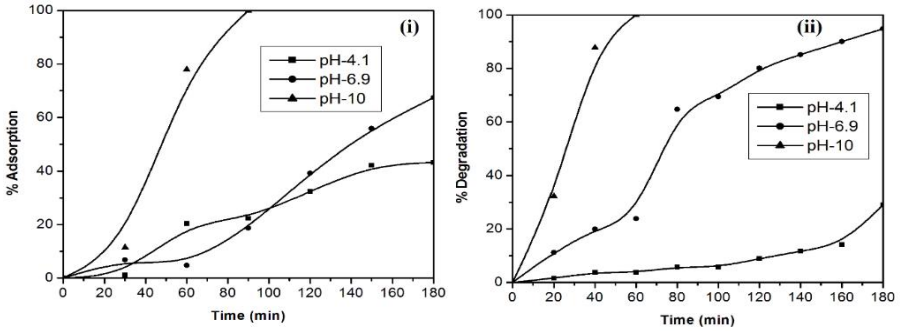

Fig.-7c: Effect of pH (i) Adsorption (ii) Degradation

Effect of Solution pH

Photocatalytic degradation of methylene blue was evaluated over a broad pH range (3-11) (Fig.-6C). Optimal performance was at pH 7.0 with 94% removal, with degradation efficiency declining to 66% at pH 3 and 69% at pH11.[1] The neutral pH optimisation for methylene blue is noteworthy since some literature reports indicate optimal MB degradation at alkaline pH (pH 12) for certain CeO_2-based systems; this difference likely reflects the particular zeolite-support environment which moderates surface charge effects. Degradation efficiency decreased substantially at both acidic and alkaline extremes, likely due to: (i) altered surface charge on catalyst affecting methylene blue adsorption behavior; (ii) changes in dye ionization state and molecular configuration affecting substrate-catalyst interactions ; (iii) pH-dependent surface hydroxyl group protonation state affecting ·OH radical generation efficiency; (iv) competing effects of excess H^+ or OH^- ions on catalytic mechanisms; and (v) reduced photocatalytic activity at extreme pH values.[1,23] The pH 7.0 optimum indicates excellent practical applicability for treating neutral industrial wastewater streams without requiring pH adjustment.

Catalyst Recyclability and Structural Stability

Catalyst recyclability is essential for practical environmental remediation applications and economic viability. CeO_2/Zeo-NaX was subjected to consecutive photocatalytic cycles for methylene blue degradation following a standardized recovery and regeneration protocol (Fig.-7): after each photocatalytic run, catalyst was recovered by high-speed centrifugation (8000 rpm, 5 min), washed sequentially with distilled water and absolute ethanol to remove adsorbed dye and aqueous species, dried at 110°C for 12 h, and calcined at 400°C for 2 h in air furnace before reuse.[1]

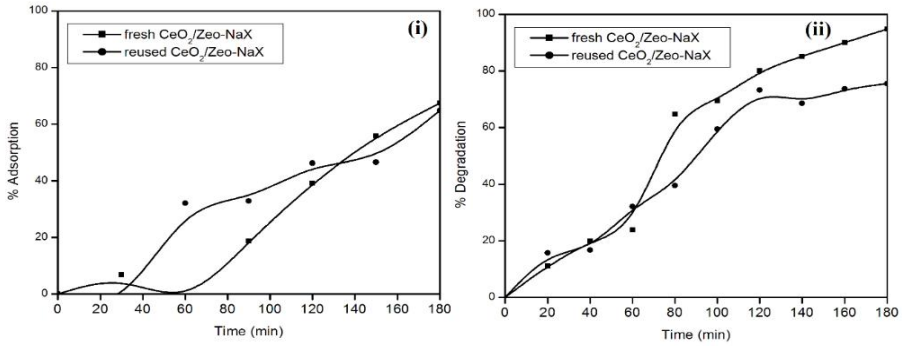

Fig.-8: Effect of Recycling the Catalyst

Methylene Blue Degradation Efficiency Over Consecutive Cycles
Initial: 94.1%
After 1st photocatalytic cycle: 90.2% (95.8% retention)
After 2nd cycle: 86.5% (91.9% retention)
After 3rd cycle: 83.7% (88.9% retention)
After 4th cycle: 83.9% (89.1% retention)

The composite photocatalyst retained approximately 89% of original catalytic efficiency for methylene blue degradation even after four consecutive photocatalytic-recovery-regeneration cycles, demonstrating acceptable and practically viable operational stability suitable for continuous water treatment operations.[1,8,26] This gradual activity decline is not unusual in practical photocatalytic systems and does not substantially compromise suitability for environmental applications where periodic catalyst regeneration can be implemented.[1,8] The performance demonstrates reliable reusability for methylene blue removal in industrial treatment scenarios. PXRD analysis and SEM examination of the spent catalyst (CeO_2/Zeo-NaX-S) after four cycles of methylene blue degradation confirmed that main structural and morphological features were preserved-crystallite sizes remained at 4.40 nm, Si/Al ratio maintained at 1.139, and cerium content at 4.82%-indicating that the material possesses robust chemical stability and can withstand repeated photocatalytic operation cycles.[1] The preservation of structural integrity after multiple methylene blue degradation cycles suggests that the material would be suitable for real-world wastewater treatment applications. The moderate activity decline observed with recycling is attributed to cumulative effects of: (i) minor leaching of cerium species during catalyst recovery and aqueous washing procedures, as evidenced by slight decrease in Ce content from 12.45% to 4.82% after four cycles; (ii) possible accumulation of non-completely-mineralized degradation intermediates (such as partially oxidized methylene blue derivatives) on catalyst surface that partially block active sites; (iii) slow photoinduced surface reconstruction and oxidation under extended light exposure; and (iv) minor structural changes during repeated drying-calcination-rehydration cycles.[1,8] These factors are common in practical heterogeneous photocatalytic systems and represent acceptable trade-offs between operational performance and economic feasibility.[1,8]

CONCLUSION

Coal fly ash was successfully converted into NaX zeolite and modified with CeO_2 nanoparticles to produce a recyclable photocatalyst for methylene blue removal. The CeO_2/Zeo-NaX composite achieved more than 94% degradation under visible light and followed pseudo-first-order kinetics with a rate constant of 0.0259 min-1. Its high surface area (94.58 m2/g), reduced band gap (2.85 eV), and nanoscale CeO_2 crystallites contributed to improved adsorption, visible-light utilisation, and charge separation. The catalyst retained approximately 89% of its initial activity after four consecutive cycles, demonstrating good reusability and structural stability. These results show that coal fly ash can be converted into a functional material for wastewater treatment while supporting resource recovery and circular-economy objectives. The study directly contributes to SDG-6, Clean Water and Sanitation. Future work should test real textile effluents, quantify mineralisation and toxicity reduction, and evaluate regeneration and continuous-flow operation.

ACKNOWLEDGMENTS

Author is grateful to the authorities of her institution for providing the basic facilities.

CONFLICT OF INTERESTS

The authors declare no conflict of interest.

AUTHOR CONTRIBUTIONS

The present work is related to *SDG-6: Clean Water and Sanitation*. The author contributed significantly to this manuscript, participated in reviewing/editing and approved the final draft for publication. The research profile of the author can be verified from her ORCID id, given below:

G. Sudha https://orcid.org/0009-0001-6239-8486

Cite this article as: G. Sudha, *Rasayan J. Chem.*, 19(3), 1890-1901(2026), https://doi.org/10.31788/RJC.2026.1939759

REFERENCES

1. H.B. Tadese, A.T. Mengesha, D.F. Tegegn, H.Z. Belachew, *BMC Chemistry*, **19**, 321 (2025), https://doi.org/10.1186/s13065-025-01686-w
2. G. Petcu, E.M. Anghel, I. Atkinson, F. Papa, N.G. Apostol, A. Baran, S. Petrescu, B. Trica, K. Tenchev, S. Todorova, V. Parvulescu, *Catalysis Today*, **459**, 115403(2025), https://doi.org/10.1016/j.cattod.2025.115403
3. B. Hazarika, B. Bhattacharjee, M. Ahmaruzzaman, *Inorganic Chemistry Communications*, **168**, 112960 (2024), https://doi.org/10.1016/j.inoche.2024.112960
4. S.N. Matussin, F. Khan, M.H. Harunsani, Y.-M. Kim, M.M. Khan, *Scientific Reports*, **14**, 8269(2024), https://doi.org/10.1038/s41598-024-58688-2
5. G. Salehi, M. Bagherzadeh, R. Abazari, M. Hajilo, D. Taherinia, *ACS Omega*, **9**, 4581(2024), https://doi.org/10.1021/acsomega.3c07326
6. S. Girma, A.M. Taddesse, Y. Bogale, Z. Bezu, *Journal of Photochemistry and Photobiology A: Chemistry*, **444**, 114963(2023), https://doi.org/10.2139/ssrn.4472059
7. X. Chen, P. Zhang, Y. Wang, W. Peng, Z. Ren, Y. Li, B. Chu, Q. Zhu, *Frontiers of Environmental Science and Engineering*, **17**, Article 149(2023), https://doi.org/10.1007/s11783-023-1749-2
8. M. Mahamud, A.M. Taddesse, Y. Bogale, Z. Bezu, *Materials Research Bulletin*, **161**, 112176(2023), https://doi.org/10.2139/ssrn.4299929
9. W. Mohammed, M. Matalkeh, R.M. Al Soubaihi, A. Elzatahry, K.M. Saoud, *ACS Omega*, **8**, 40063(2023), https://doi.org/10.1021/acsomega.3c01766
10. N. Bux, S.H. Tumrani, R.A. Soomro, X. Ji, *International Journal of Economic and Environmental Geology*, **13**, 58(2022), https://doi.org/10.46660/ijeeg.v13i2.32
11. M.F. Mubarak, E.A. Kamoun, M.Y. Nassar, T. Mahmoud, *RSC Advances*, **16**, 23895(2026), https://doi.org/10.1039/D6RA00287
12. P. Thuadaija, A. Nuntiya, *ScienceAsia*, **38,** 295(2012), https://doi.org/10.2306/scienceasia1513-1874.2012.38.295
13. T.P. Amaladhas, S.S. Thavamani, *Advanced Materials Letters*, **4**, 688(2013), https://doi.org/10.5185/amlett.2013.1406
14. G. Hu, J. Yang, X. Duan, R. Farnood, C. Yang, J. Yang, W. Liu, Q. Liu, *Chemical Engineering Journal*, **417,** 129209(2021), https://doi.org/10.1016/j.jallcom.2025.181573
15. S. Wang, J. Yun, B. Luo, T. Butburee, P. Peerakiatkhajohn, S. Thaweesak, M. Xiao, L. Wang, *Journal of Materials Science and Technology*, **33**, 1(2017), https://doi.org/10.1016/j.jmst.2016.11.017
16. K. Ahmad, H.R. Ghatak, S.M. Ahuja, *Environmental Technology and Innovation*, **19**, 100893(2020), https://doi.org/10.1016/j.eti.2020.100893

17. N. Kanmaz, *Journal of Industrial and Engineering Chemistry*, **157**, 822(2026), https://doi.org/10.1016/j.jiec.2026.03.019
18. E.A. Mohamed, A.A. Altalhi, H.M. Ahmed, N.A. Negm, *Desalination and Water Treatment*, **324**, 101539(2025), https://doi.org/10.1016/j.dwt.2025.101539
19. L.J. Kusumawardani, T. Widdyanti, A. Iryani, U. Hasanah, N. Nurlela, *Sains Natural*, **14**, 98(2024), https://doi.org/10.31938/jsn.v14i2.722
20. A. Jankowska, R. Panek, W. Franus, J. Goscianska, *Molecules*, **29**, 5244(2024), https://doi.org/10.3390/molecules29225244
21. X. Ren, R. Qu, S. Liu, H. Zhao, W. Wu, H. Song, C. Zheng, X. Wu, X. Gao, *Aerosol and Air Quality Research*, **20**, 1127(2020), https://doi.org/10.4209/aaqr.2019.12.0651
22. V. Gadore, S.R. Mishra, N. Yadav, G. Yadav, M. Ahmaruzzaman, *Inorganic Chemistry Communications,* **166**, 112606(2024), https://doi.org/10.1016/j.inoche.2024.112606
23. C. Yang, W. Lee, C.-C. Chen, *RSC Advances*, **6,** 40664(2016), https://doi.org/10.1039/C6RA02299E
24. K. Ralphs, J. Liu, L. Lan, C. Hardacre, N. Skillen, P.K.J. Robertson, *RSC Sustainability*, **3**, 2079(2025), https://doi.org/10.1039/D4SU00646A
25. S. Dogar, S. Nayab, M.Q. Farooq, A. Said, R. Kamran, H. Duran, B. Yameen, *ACS Omega*, **5**, 15850(2020), https://doi.org/10.1021/acsomega.0c00889
26. Y. Sun, D.W. O'Connell, *Water Environment Research*, **94,** e10781(2022), https://doi.org/10.1002/wer.10781
27. S. Modi, V.K. Yadav, D. Ali, N. Choudhary, S. Alarifi, D.K. Sahoo, A. Patel, M.H. Fulekar, *Water,* **15**, 3915(2023), https://doi.org/10.3390/w15223915
28. M.R. Islam, B. Biswas, R. Naidu, *ACS Sustainable Resource Management*, **1,** 799(2024), https://doi.org/10.1021/acssusresmgt.4c00033

[RJC-9759/2026]